Published in final edited form as:

J Biomed Mater Res B Appl Biomater. 2020 July ; 108(5): 2238–2249. doi:10.1002/jbm.b.34561.

Micro-CT and histopathology methods to assess host response of aneurysms treated with shape memory polymer foam-coated coils versus bare metal coil occlusion devices

Staci L. Jessen[1,2], **Molly C. Friedemann**[1], **Annmarie E. Mullen**[2], **Anne-Marie Ginn-Hedman**[2], **Scott M. Herting**[2], **Duncan J. Maitland**[2], **Fred J. Clubb Jr**[1,2]

[1]Department of Veterinary Pathobiology, Texas A&M University, College Station, Texas

[2]Department of Biomedical Engineering, Texas A&M University, College Station, Texas

Abstract

Recent studies utilizing shape memory polymer foams to coat embolizing coils have shown potential benefits over current aneurysm treatments. In the current study utilizing a rabbit-elastase aneurysm model, the performance of test article (foam-coated coil [FCC]) and control (bare platinum coils [BPCs]) devices were compared at 30, 90, and 180 days using micro-CT and histological assessments. The host response was measured by identifying the cells regionally present within the aneurysm, and assessing the degree of residual debris and connective tissue. The 3D reconstructions of aneurysms provided context for histologic findings, and aided in the overall aneurysm assessment. At all time points, >75% of the cells categorized in each aneurysm were associated with a bioactive yet biocompatible host response (vs. the remainder of cells that were associated with acute inflammation). The extracellular matrix exhibited a transition from residual fibrin at 30 days to a greater degree of connective tissue at 90 and 180 days. Although the control BPC-treated aneurysms exhibited a greater degree of connective tissue at the earliest time point examined (30 days), by 180 days, the FCC-treated aneurysms had more connective tissue and less debris overall than the control aneurysms. When considering cell types and extracellular matrix composition, the overall host response scores were significantly better in FCC-treated aneurysms at the later time point. Based on the results of these metrics, the FCC device may lead to an advanced tissue remodeling response over BPC occlusion devices.

Keywords

healing metric; histopathology; micro-CT; occlusion devices; shape memory polymer

Correspondence Duncan J. Maitland, Department of Biomedical Engineering, Texas A&M University, 3120 TAMU, College Station, TX. djmaitland@tamu.edu.

CONFLICT OF INTEREST

The authors disclose that Dr. Fred Clubb and Dr. Duncan Maitland hold stock in a company, Shape Memory Medical, Inc. (Santa Clara, CA, shapemem.com), that is commercializing the foam-over-coil technology featured in this manuscript. Further, Dr. Maitland is a Director and Chief Technology Officer at Shape Memory Medical, Inc.

1 | INTRODUCTION

1.1 | Intracranial aneurysms

Despite major advances in the world of medicine, intracranial aneurysms remain a health risk for many patients worldwide. Aneurysms can form when the wall of an artery weakens, allowing the vessel wall to balloon outward, and if left untreated, can potentially rupture, resulting in a debilitating or fatal hemorrhage. In the United States alone, approximately 1 in 50 adults have unruptured intracranial aneurysms, and 30,000 ruptures occur each year (Molyneux, Birks, Clarke, Sneade, & Kerr, 2015).

1.2 | Treatment options

Several treatment options have been developed to prevent aneurysmal rupture, some of which focus on preventing further blood flow into the aneurysm dome, reducing the stress and pressure on the artery wall and promoting clot formation. Treatments involving occlusion devices prevent rupture mechanistically by isolating the aneurysm from parent artery flow. Rodriguez et al. (2015) discusses a comprehensive review of aneurysm occlusion devices, including the minimally-invasive method of introducing embolizing coils (bare platinum coils [BPCs]) through an angiography-guided endovascular catheter.

While embolic coils have emerged as a popular treatment option, complications associated with this method remain, which include recanalization, unorganized thrombus formation and poor aneurysm healing, low volume occlusion leading to compacted coils from pulsing arterial flow, and failure to form neointimal layers in the aneurysm neck. These complications can result in aneurysm growth/rupture and daughter aneurysm formation. The current coiling procedure also risks coil migration into the parent artery as well as artery puncture during coil placement. These potential complications demonstrate the need for advancement in coiling devices to improve aneurysm treatment outcomes (Brinjikji, Kallmes, & Kadirvel, 2015).

The use of shape memory polymer (SMP) foams has been documented in various intravascular devices (Boyle, Landsman, Wierzbicki, et al., 2016; Horn et al., 2017; Landsman et al., 2016; Rodriguez et al., 2014; Wierzbicki, Bryant, Miller, Keller, & Maitland, 2016). To address shortcomings with the BPCs, the Biomedical Device Laboratory at Texas A&M University developed a foam-coated coil (FCC) device as a new option for aneurysm treatment. In a recent study, Herting et al. demonstrated that the FCC device in a rabbit elastase model elicited a greater degree of neointimal thickening in the aneurysm neck and an overall greater packing density when compared to aneurysms treated with BPCs (Herting et al., 2019). Although the aneurysms treated with FCCs reported statistically insignificant increased rates of recanalization, the FCC device overall shows potential to improve outcomes of aneurysm treatment. In this manuscript, we introduce micro-CT evaluation and additional histopathology assessments to further define the stages of healing within the rabbit-elastase model aneurysms described previously by Herting et al., and compare the healing characteristics of FCC and BPC devices.

2 | MATERIALS AND METHODS

2.1 | Animal model

All animal study methods were approved by the Mayo Clinic IACUC and conducted according to AUP# A68514-15-R17 with oversight by the principal institution for this study, Texas A&M University (AUP# 2017-0430 EX). The animal study was performed at the Mayo Clinic in Rochester, MN. Aneurysms were created in New Zealand White Rabbits by isolating a portion of the right common carotid artery and exposing it to a porcine elastase enzyme to break down the vessel wall as has been described previously (Altes et al., 2000). After aneurysms had been allowed to grow for at least 3 weeks, aneurysms were treated using either FCC device prototypes or BPC controls. A detailed procedure was presented by Herting et al. (2019). Briefly, the animal was assigned to a device treatment group before visualization of the aneurysm (animal study design; Table 1). Sterile technique was used to gain access to the femoral artery, then a microcatheter was inserted and positioned outside of the aneurysm. Digital subtraction angiography (DSA) was performed to assess the size of the aneurysm by comparison to radiopaque markers and to guide the delivery of devices. Measurements of the greatest width across the aneurysm and the length from the aneurysm neck to the dome were made on the DSA images, and, assuming an ellipsoid geometry, the pretreatment aneurysm volume (measured in mm^3) was calculated using the equation,

$$\text{Volume} = \frac{\pi \mid w^2}{6}$$

where w is the width of the aneurysm (measured in mm), and l is the length from the aneurysm neck to the dome (measured in mm). After aneurysm size assessment, multiple SMP FCCs or multiple BPCs were delivered, then treatment was stopped at the discretion of the experienced interventionalist; treatment was stopped either when the coil packing was satisfactory for a clinical case, or when the delivery of additional devices would risk leaving coil loops in the parent artery. A final DSA was performed, then the animals were taken to recovery. Animals were housed in pairs until the designated time point for euthanasia, which was at 30, 90, or 180 days post device implantation (Table 1). DSA was also performed at the time of sacrifice to visualize the stability of the treatment. The aneurysm was then explanted and submerged in 10% neutral buffered formalin at a 10:1 fixative to tissue volume ratio.

2.2 | Postexplant micro-CT evaluation

After explantation, formalin-fixed aneurysms were photographed grossly and then micro-CT scanned within a North Star Imaging X50 machine (Rogers, Minnesota) at the Cardiovascular Pathology Laboratory at Texas A&M University (CVP-TAMU). Aneurysms were then shipped back to the Mayo Clinic for slide preparation and analysis (Herting et al., 2019). Micro-CT was performed (prior to sectioning for histology) to provide the original 3D orientation of the coils within the aneurysm for reference during histology analysis. Scanning parameters were optimized for each specimen, with resolutions ranging from ~4.4–12.1 μm. The scans were then reconstructed with Wallis filters of varying intensities to delineate the coil-tissue interface within the three-dimensional view. Postexplant aneurysm

volumes were calculated from the micro-CT scans using a simple region-growing segmentation algorithm within 3D Slicer (Fedorov et al., 2012; Kikinis, Pieper, & Vosburgh, 2014). Additionally, in correlation with the histology (discussed below), these 3D reconstructions were used to examine presence of coils within the parent artery lumen or in the adventitial layer of the aneurysm wall.

2.3 | Histopathology evaluation

Formalin-fixed tissues were processed for histology as described in Herting et al. (2019) by the Mayo Clinic. Briefly, tissues were dehydrated in ascending concentrations of ethanol, cleared with xylene, and then embedded in paraffin wax. The resulting tissue blocks were sectioned to 1 mm blocks in a coronal orientation using an Isomet Low Speed saw, and the metal coil fragments from each device were removed using forceps under a dissection microscope. The 1 mm thick sections were reembedded in paraffin without the coil fragments, and these new blocks were cut to 4 μm sections using a microtome. The sections were stained with either hematoxylin and eosin (H&E) or Masson's Trichrome for histological evaluation. Finally, the slides were shipped to CVP-TAMU for the studies in this manuscript.

H&E and Trichrome-stained glass slides containing the mid-sagittal cross-sections from each aneurysm treated with the test device (FCC) and control device (BPC) were oil-immersion scanned with a ×100 objective on the Olympus VS120 Virtual Microscope (Tokyo, Japan) at CVP-TAMU; slides were viewed and analyzed using the OlyVia iPad application. The histology analysis was not blinded as the control and test article were morphologically distinct due to the presence of foam in the test article. Trichrome-stained sections were used to evaluate the extent of connective tissue and residual fibrin that makes up the extracellular matrix within each aneurysm (Table 2). Inflammation was evaluated for each aneurysm using the metric defined in Table 3; individual inflammatory cells were counted in multiple high power fields (HPFs, defined as ~0.01 mm^2) across each aneurysm. Inflammatory cell types identified and counted include heterophils, lymphocytes, eosinophils, and macrophages (including instances of erythrophagocytosis and hemosiderin-laden macrophages). This method of counting inflammatory cell types based on well-established morphologic features has been used previously in evaluation of intravascular devices (Horn et al., 2017; Jessen et al., 2019). An inflammatory cell total (I_T) was calculated for each aneurysm as the average number of total inflammatory cells per HPF. Additionally, a modified inflammatory cell total (I_M) was calculated for each aneurysm, which included only inflammatory cells associated with acute inflammation (i.e., heterophils, lymphocytes, and eosinophils). Based on these totals (I_T and I_M), each aneurysm was assigned an inflammation score and a modified inflammation score (ranging from 0 to 4, Table 3) in order to perform a nonparametric statistical analysis on these parameters. Additionally, each HPF was assigned a debris score based on the metric in Table 2. The number of HPFs analyzed per aneurysm depended on the overall size of the aneurysm. However, within each aneurysm, multiple HPFs were analyzed in the outer region (including the aneurysm neck), and the mid and inner regions (Figure 1). Finally, based on inflammation, neovascularization, and content of the extracellular matrix, each aneurysm was given an overall tissue response score (defined in Table 4). This metric has been

previously used and validated in another intravascular occlusion device (Jessen et al., 2019). When H&E stained slides were suspected to show possible coils in the parent artery lumen, the 3D reconstruction was analyzed as 2D axial slices to compare the orientation of the coils *en bloc* and confirm whether coils were within the lumen, or if the displaced tissue was a histological processing artifact.

2.4 | Statistical analysis

Differences in aneurysm volume from pretreatment to postexplant time points were analyzed using a matched pairs *t*-test (i.e., each aneurysm's volume before and after treatment were treated as matched pairs, and the mean differences in volume were compared across treatment groups at each time point). Average inflammatory cells counted per HPF were analyzed using an independent t-test. The assigned inflammatory, debris, fibrin, connective tissue, and overall tissue response scores were analyzed with the Wilcoxon/Kruskal–Wallis nonparametric test. All statistical analyses were performed with 95% confidence intervals.

3 | RESULTS

Overall, upon explant, there were no appreciable gross differences between the FCC- and BPC-treated aneurysms; each aneurysm was irregularly shaped with a translucent pseudo-intimal coating over the coils (Figure 2). In some aneurysms, the coils are visible through the aneurysm wall (Figure 2: 90.FCC, 180.BPC, and 180.FCC); micro-CT scans reveal coil placement within the aneurysm dome with a noticeable layer of tissue covering the coils, which is verified by the corresponding histological cross-section (Figure 2). Two aneurysms implanted with the FCC device exhibited histologic evidence of a focal rupture with coil extending into the adventitia, however, there was no secondary extravasation at this site in either aneurysm. By analyzing the 2D cross-sections of each micro-CT reconstruction compared to the histology (Figure 3), coils were apparent in the parent artery of 15 out of 56 aneurysms (11 implanted with the test article and 4 implanted with the control); this is presumed due to the implant procedure.

3.1 | Aneurysm volume

The aneurysm pretreatment volume ranged from 13.91 to 344.77 mm^3 (average of 81.9 ± 71.7 mm^3), and the postexplant volume ranged from 13.6 to 298.2 mm^3 (average of 73.4 ± 62.3 mm^3). The percent volume decrease in aneurysm size varied across time points for test and control groups (Figure 4), and there were no significant differences among treatment groups in the average pretreatment and postexplant volume changes at any time point.

3.2 | Inflammation

The average inflammatory cells per HPF and corresponding inflammation scores for each time point and device type are listed in Table 5. At 30 and 180 days, there were no significant differences in the total number of inflammatory cells per HPF between the two device types. At 90 days, the average total number of inflammatory cells were significantly higher in the FCC-treated aneurysms; however, when only considering the inflammatory cells associated with acute inflammation (heterophils, eosinophils, and lymphocytes), there were no significant differences between the two device types at all time points (I_M, Table 5).

At all time points, the modified inflammation score was at least 1–2 points lower than the total inflammation score, meaning that the majority of the classified inflammatory cells present across the aneurysms were macrophages. Across all time points, there are no significant differences in the modified inflammation scores between the two device types.

The breakdown of cell types in each region throughout the aneurysm dome (outer, mid, and inner; see Figure 1) is displayed in Figure 5. At all time points, approximately >75% of cells counted within each aneurysm region were associated with healing (macrophages, erythrophagocytosis, and hemosiderin-laden macrophages). At 30 days, the inner region of aneurysms treated with BPC and FCC exhibited more cells typically seen in acute inflammation (eosinophils, lymphocytes, and heterophils) when compared to the inner region at later time points; however, there was no significant difference between the total number of acute inflammatory cells in the FCC-treated aneurysms compared to the controls.

Figure 6 displays a cross-section of an example 30-day FCC-treated aneurysm. Regionally, areas of increased acute inflammation are apparent near the neck of the aneurysm (Figure 6; red inset). There are also regions of increased healing apparent mostly toward the outer region of the aneurysm (Figure 6; blue inset). At 30 days, it is apparent that the foam struts remain within the aneurysm, with mild infiltration of fibrin within the extracellular matrix (Figure 7, top). By 90 days (Figure 7, middle), the foam has mostly degraded and areas of acute inflammatory reactions have begun to resolve with increased areas of collagen deposition. By 180 days, the foam is rarely present, and most areas of the aneurysm have transitioned toward healing (mostly macrophages present; Figure 7, lower). BPC-treated aneurysms exhibit a similar cellular response (Figure 8).

3.3 | Extracellular matrix assessment

Connective tissue, residual fibrin, and debris scores are displayed in Figure 9 and defined in Table 2. In this assessment, debris included cellular necrosis, residual fibrin, and hemorrhage. At the 30 day time point, BPC-treated aneurysms exhibited significantly greater connective tissue coverage over the FCC-treated aneurysms. However, at 90 days, all of the aneurysms showed 75–100% connective tissue coverage, and at 180 days, the FCC-treated aneurysms exhibited significantly greater connective tissue coverage compared to the BPC group. Fibrin scoring revealed a similar pattern; on average, greater amounts of residual fibrin were observed for FCC-treated aneurysms at 30 days, but these differences were not significant. However, at 90 days fibrin was rarely observed in either treatment group. At 180 days, FCC-treated aneurysms showed significantly lower fibrin content in the mid and inner regions compared to BPC-treated aneurysms. The degree of total debris within the aneurysm dome also declined over time for both device types. The 30 and 90 day time point showed no significant difference between the debris content of FCC- and BPC-treated aneurysms; however, at 180 days there were significantly lower amounts of debris in FCC-treated aneurysms.

3.4 | Tissue response

At 30 and 90 days, there were no significant differences between the average tissue response scores of FCC- and BPC-treated aneurysms (Figure 10). However, at 180 days, the FCC-

treated aneurysms show a significantly improved tissue response score in all regions of the aneurysm when compared to the BPC-treated aneurysm at this time point. Overall, the test article (FCC) trends toward an earlier maturation process in healing versus the control (BPC), with the greatest degree of remodeling in the outer region.

4 | DISCUSSION

4.1 | Use of micro-CT in aneurysm assessment

Postexplant aneurysm evaluation is typically limited to a histological evaluation. While histologic sections provide useful information about device-tissue interactions on a cellular level, micro-CT of tissues with medical devices prior to histological sectioning can provide invaluable context, as it provides a nondestructive, slice-by-slice view of the specimen's complete volume (Friedemann et al., 2019; Loos, Rohde, Haverich, & Barlach, 2007; Opie et al., 2017), and has become a useful tool to aid a histologic evaluation (Langheinrich et al., 2005; Rousselle & Wicks, 2008). In this study, the 3D reconstruction allows visualization of coil positioning (e.g., proper placement vs. implantation artifact) relative to the aneurysm dome and parent artery that may prove difficult histologically, due to the destructive nature of the histologic sectioning. Because paraffin histology requires removal of the metal components that might inherently induce sectioning artifact, evaluating the histology sections alone can leave some ambiguity as to whether or not the coils were exposed either in the lumen of the parent artery or outside the aneurysm sac (as some coils were visible externally; recall Figure 2). The micro-CT scans reconstructed with an appropriate filter allowed for delineation of the tissue from the metal device components, and coil placement within the aneurysm was able to be assessed en *bloc* (Figure 3). This method utilizing micro-CT prior to histology accommodated confirmation of presence/absence of coils in the parent artery lumen or protrusion of coils through the aneurysm wall externally. However, micro-CT scans of metal components can produce significant beam hardening artifact that can limit interpretation. In all cases, but especially in cases where beam hardening was significant, micro-CT assessment was correlated with histological cross-sections to confirm findings (Figure 3). In aneurysms where coils were grossly visible, the micro-CT and histology cross-sections confirm a tissue covering over all coils within the aneurysm dome; two aneurysms in this study exhibited coils extending into the adventitia, but there was no appreciable extravasation at these sites. These focal, isolated occurrences can be considered procedural, and the lack of extravasation indicates the ability of the device to provide sufficient hemostasis. In the animals where coils were present within the lumen of the parent artery (also related to the implant procedure), there was no evidence of active thrombogenesis involving exposed coils. Furthermore, these coils within the lumen did not produce any gross or microscopic evidence of downstream thromboembolic occlusion. Plus, further validation by *in vivo* analysis showed that all animals (treatment and control groups) were clinically normal throughout the study.

4.2 | Tissue remodeling and healing

The characterization of a host's response to an intra-aneurysmal device is an important component of assessing safety and provides a method to directly compare treatment options. The ideal host response to an intra-aneurysmal device consists of four main steps: initial clot

formation, inflammation, proliferation, and eventual remodeling. The goal of this study is to assess the host response by correlating information gleaned from *in situ* evaluation via gross evaluation and micro-CT (Rousselle & Wicks, 2008), and histologic evaluation of the device-tissue interface (Friedemann et al., 2019).

An intra-aneurysmal device activates the body's intrinsic and extrinsic coagulation pathways to form a fibrin blood clot within the aneurysm (Brinjikji et al., 2015; Horn, Maitland, Hartman, & Ortega, 2018); this is the first step in the host response, followed by inflammation. Inflammation is a beneficial host reaction to non-native tissue that involves clearing fibrin, injured tissue and/or foreign components (eliciting a foreign body response) (Kumar, Abbas, & Aster, 2018). In the acute phase of inflammation/healing, humoral and cellular components (leukocytes, including heterophils, eosinophils, lymphocytes, and eventually macrophages) are recruited to the area for removal of the foreign material (in the case of a foreign body response), or removal of the initial fibrin-enmeshed blood clot formed immediately after the injury (or in the case of intravascular devices, immediately after implant). Chronic inflammation can involve the continual recruitment of leukocytes to the area and either transitions to sustained tissue injury, and/or remodeling/healing (i.e., deposition of immature granulation tissue). Over time there is progression to the proliferation phase, where mature, dense connective tissue begins to form; throughout this process, the tissues may contract as the connective tissue matrix progresses from a loose to a dense collagen network. Finally, the remodeling phase results in the final dense, acellular scar tissue formation. In terms of aneurysm treatment with an occlusion device, the ideal response involves tissue remodeling, which refers to transition to a collagen-based extracellular matrix that permanently occludes the aneurysm (Velnar, Bailey, & Smrkolj, 2009). The tissue remodeling response of ECM contraction has been described in previous foam-based aneurysm occlusion studies. In fact, in a previous study of porcine side-wall aneurysms described by Horn et. al, there was a collagen-dense connective tissue matrix that exhibited a noticeable decrease in aneurysm size after 180 days of treatment with a foam-only occlusion device (Horn et al., 2017).

Using the metrics defined in this study, the aneurysms treated with BPCs and FCCs each exhibited a progressive remodeling response from transition of the initial fibrin-enmeshed blood clot at implant to a dense collagen matrix. This remodeling due to a foreign body response (vs. injury response) is reflected by the higher tissue response scores at 30 days and the lower scores at 180 days (Figure 10), in conjunction with the absence of necrosis and the increase in connective tissue deposition at the later time point. The low tissue response scores at 90 days (correlating to more advanced healing) can be attributed to the lower sample size of 90 day aneurysms compared to the other time points. These findings reflect results by Herting et al., that showed a progressive increase in collagen deposition over time (for both FCC- and BPC-treated aneurysms) when measuring the percent area covered by collagen throughout the entire histologic cross-section. The method for extracellular assessment described in the current paper differs by qualitatively separating loose and dense collagen (tissue response score; Figure 10), and also including the degree of residual fibrin and debris in the overall assessment (Figure 9).

Despite evidence of tissue remodeling, unlike previous aneurysm studies involving shape memory foam, the tissue contraction was not significant (Figure 4). This is presumed due to the physical barrier provided by the metal coils in both the test and control groups. Additionally, the central region of the aneurysm domes progressed to an advanced tissue response score much slower than the outer regions of the aneurysm domes. The coils, in addition to preventing the decrease in size of aneurysm as host response progressed, may have provided a barrier that slowed the migration of macrophages to the central region to clear out the initial blood clot and recruit fibroblasts for deposition of collagen into the extracellular matrix.

Control aneurysms treated with BPCs exhibited the expected response according to published literature. Rabbit elastase aneurysms treated with bare coils typically result in loose, hypocellular tissue healing/remodeling in the dome. Cell types observed generally include chronic inflammatory cells and some giant cells. Aneurysm contraction has not yet been reported, and the neck is usually only covered by a single layer of endothelial cells (Brinjikji et al., 2015; Dai et al., 2005; Dai, Ding, & Lewis, 2006).

4.3 | Acute versus chronic inflammation

During a histological evaluation of inflammation, it is important to morphologically distinguish the types of leukocytes at the implant site, as each cell type has a different role. Additionally, macrophages can be activated by different signals to move forward in two distinct pathways. Classically activated macrophages play a major role in the continual recruitment of inflammatory cells to the area, which can lead to chronic, sustained inflammation. Alternatively-activated macrophages, activated by leukocyte cytokines, are involved in the recruitment of fibroblasts and transition to collagen deposition (Anderson, Rodriguez, & Chang, 2008). Neutrophils and eosinophils, on the other hand, are inflammatory cells involved mostly in active inflammation, and although typically active most within the 48 hour window after injury, their presence may persist (Kumar et al., 2018; Velnar et al., 2009). In this paper, we have established a method of assessing the stages of inflammation and transition to healing by distinguishing and quantifying the type of leukocytes present in regions throughout the aneurysm dome. In doing so, we have a better sense of whether or not the host response to the device is remodeling and transitioning toward a healing response. This quantitative assessment comparing three circumferential regions throughout the dome builds upon and adds to the inflammation assessment described by Herting et al. (2019), which focused solely on a qualitative assessment that regionally only compared inflammation at the aneurysm dome and wall across groups.

In this study, the 30 day time point is an important transition phase as exhibited by the inflammatory cells associated with acute inflammation (Figure 5) and concurrent macrophage-directed transitioning to a sustained collagen/vascular based remodeling to granulation tissue. By 90 days, acute inflammatory cells are less frequent, and have been replaced by macrophages breaking down the embedded erythrocytes within cross-linked fibrin (erythrophagocytosis, transitioning to hemosiderin-laden macrophages), and fibroblasts producing collagen. This reflects the established timeline for classic remodeling and cellular healing (Kumar et al., 2018; Velnar et al., 2009). Where Herting et al. showed

increased inflammatory cell infiltration at the aneurysm dome (compared to the aneurysm wall) for both device types (with the exception of the FCC group at 30 days), the methods described in this study (quantifying the cell types seen in each region of the dome [outer, middle, and inner]) revealed that the aneurysm displays a trend of healing/remodeling that begins in the outer regions and progresses inward over time.

4.4 | Necrotic debris

As the goal of the host response during medical device implantation is to replace the initial blood clot and fibrin with mature, dense connective tissue, a degree of cellular necrosis is expected during this process; this is a response to local tissue hypoxia and mechanical cellular injury that naturally follows device implantation. This necrosis is one of the instigators of leukocyte recruitment, which phagocytize the debris and eventually leads to the transition to mature collagenous connective tissue. Higher debris scores at 30 days are expected and correspond to areas of cellular necrosis, fibrin, and hemorrhage in both the test and control aneurysms. Lower debris scores at 90 and 180 days are a direct reflection of a transition to mature connective tissue extracellular matrix and indicates that there is no sustained necrosis at later time points. This further demonstrates the transition to remodeling and healing of the aneurysms.

4.5 | Limitations

The coils in both test and control groups exhibit mononuclear to multinuclear cellular response; however, the coils were manually removed from the specimens prior to paraffin embedding, which led to extensive artifact in some specimens, as the extracellular matrix was infiltrated within the coils. In some cases, the surrounding tissue was removed along with the coils, which precluded consistent assessment adjacent to areas of coils. Therefore, the cellular evaluation in this study was limited to areas away from the coils (i.e., not immediately adjacent to the coils).

Other limitations to this study involve the use of the elastase animal model, and the small sample size at 90 days. In this study, the elastase model provided a wide range of aneurysm sizes and shapes that were inconsistent across groups and time points. The pretreatment aneurysm volume was estimated based on an ellipsoid geometry assumption. This method for estimating aneurysm volume was not possible at explant (or at any time after coil deployment), because the coils prevented flow of contrast to the aneurysm, and any volume attained would be reflective of coil volume rather than the aneurysm sac. Thus, postexplant volumes were calculated from the micro-CT scans. Segmenting the aneurysm wall throughout the 3D reconstruction provided a more accurate method for determining aneurysm volume of irregular shape, rather than assuming ellipsoid geometry and estimating 3D volume from a 2D angiograph image. This difference in methodology, along with the fact that all tissues exhibit some degree of shrinking postmortem and with formalin fixation (Eisenberg & Mobley, 1975), makes the aneurysm volume decreases difficult to interpret. However, it is not feasible to perform a micro-CT of aneurysms *in vivo* at any time point, as the x-ray exposure would be too great, and clinical CT scans would not provide a comparable resolution as the micro-CT.

5 | CONCLUSION

Overall, the results of the micro-CT and additional histopathology methods in this manuscript reveal that the SMP FCCs show the potential to provide an advanced degree of healing within aneurysms over the BPCs. Micro-CT of aneurysms prior to histologic sectioning can provide invaluable context for histologic findings and provide a more accurate means of assessing aneurysm volume, to further assess the degree of aneurysm remodeling and healing. Additionally, the histologic approach to aneurysm assessment described in this paper can build upon traditional methods (described by Herting et al. (2019)), by providing a quantitative assessment of the cellular response regionally across the aneurysm, and distinguishing the different stages of host response in terms of extracellular matrix development (residual blood clot, loose collagen, to mature dense collagen).

In conclusion, due to the complexity of and numerous signals involved in the healing process, the method described in this paper for assessing remodeling and healing histologically by distinguishing the types of cells regionally present and the content of the extracellular matrix is important for clearly delineating acute and chronic inflammatory events from residual inflammatory activity due to the initial implant that is transitioning to healing.

ACKNOWLEDGMENT

This work was supported by the NIH National Institute of Neurological Disorders and Stroke grant U01-NS089692. This project was also supported in part by a fellowship award through the National Defense Science and Engineering Graduate (NDSEG) Fellowship Program, sponsored by the Air Force Research Laboratory (AFRL), the Office of Naval Research (ONR), and the Army Research Office (ARO).

Funding information

National Institute of Neurological Disorders and Stroke, Grant/Award Number: U01-NS089692; U.S. Department of Defense; Army Research Office; Office of Naval Research; Air Force Research Laboratory; National Defense Science and Engineering Graduate

REFERENCES

Altes TA, Cloft HJ, Short JG, DeGast A, Do HM, Helm GA, & Kallmes DFA (2000). Creation of saccular aneurysms in the rabbit: A model suitable for testing endovascular devices. American Journal of Roentgenology, 174, 349–354. [PubMed: 10658703]

Anderson JM, Rodriguez A, & Chang DT (2008). Foreign body reaction to biomaterials. Seminars in Immunology, 20, 86–100. [PubMed: 18162407]

Boyle AJ, Landsman TL, Wierzbicki MA, Nash LD, Hwang W, Miller MW, … Maitland DJ (2016). In vitro and in vivo evaluation of a shape memory polymer foam-over-wire embolization device delivered in saccular aneurysm models. Journal of Biomedical Materials Research. Part B, Applied Biomaterials, 104B, 1407–1415.

Brinjikji W, Kallmes DF, & Kadirvel R (2015). Mechanisms of healing in coiled intracranial aneurysms: A review of the literature. American Journal of Neuroradiology, 36, 1216–1222. [PubMed: 25430855]

Dai D, Ding YH, Danielson MA, Kadirvel R, Lewis DA, Cloft HJ, & Kallmes DF (2005). Histologic and immunohistochemical comparison of human, rabbit, and swine aneurysms embolized with platinum coils. American Journal of Neuroradiology, 26, 2560–2568. [PubMed: 16286401]

Dai D, Ding YH, Lewis DA, & Kallmes DF (2006). A proposed ordinal scale for grading histology in elastase-induced, saccular aneurysms. American Journal of Neuroradiology, 27, 132–138. [PubMed: 16418372]

Eisenberg BA, & Mobley BA (1975). Size changes in single muscle fibers during fixation and embedding. Tissue & Cell, 7(2), 383–387. [PubMed: 49940]

Fedorov A, Beichel R, Kalpathy-Cramer J, Finet J, Fillion-Robin J-C, Pujol S, … Kikinis R (2012). 3D slicer as an image computing platform for the quantitative imaging network. Magnetic Resonance Imaging, 30 (9), 1323–1341 PMC3466397. [PubMed: 22770690]

Friedemann MC, Mehta NA, Jessen SL, Charara FH, Ginn-Hedman AM, Kaulfus CN, … Weeks BR (2019). Introduction to currently applied device pathology. Toxicologic Pathology, 47(3), 221–234. [PubMed: 30844339]

Herting SM, Ding Y, Boyle AJ, Dai D, Nash LD, Asnafi S, … Maitland DJ (2019). In vivo comparison of shape memory polymer foam-coated and bare metal coils for aneurysm occlusion in the rabbit elastase model. Journal of Biomedical Materials Research. Part B, Applied Biomaterials, 107, 2466–2475. 10.1002/jbm.b.34337 [PubMed: 30775843]

Horn J, Hwang W, Jessen SL, Keller BK, Miller MW, Tuzun E, … Maitland DJ (2017). Comparison of shape memory polymer foam versus bare metal coil treatments in an in vivo porcine sidewall aneurysm model. Journal of Biomedical Materials Research. Part B, Applied Biomaterials, 105, 1892–1905. [PubMed: 27255687]

Horn JD, Maitland DJ, Hartman J, & Ortega JM (2018). A computational thrombus formation model: Application to an idealized two-dimensional aneurysm treated with bare metal coils. Biomechanics and Modeling in Mechanobiology, 17, 1821–1838. 10.1007/s10237-018-1059-y [PubMed: 30074100]

Jessen SL, Friedemann MC, Ginn-Hedman AM, Graul LM, Jokerst S, Robinson CB … Maitland DJ (2019). Microscopic assessment of healing and effectiveness of a foam-based peripheral occlusion device. ACS Biomaterials Science & Engineering. 10.1021/acsbiomaterials.9b00895

Kikinis R, Pieper SD, & Vosburgh K (2014). 3D slicer: A platform for subject-specific image analysis, visualization, and clinical support In Jolesz FA (Ed.), Intraoperative Imaging Image-Guided Therapy (Vol. 3, pp. 277–289). Springer, New York, NY.

Kumar V, Abbas AK, & Aster JC (2018). Inflammation and repair Robbins basic pathology (10th ed., pp. 57–95). Pennsylvania: Elsevier.

Landsman TL, Bush RL, Glowczwski A, Horn J, Jessen SL, Ungchusri E, … Maitland DJ (2016). Design and verification of a shape memory polymer peripheral occlusion device. Journal of the Mechanical Behavior of Biomedical Materials, 63, 195–206. [PubMed: 27419615]

Langheinrich AC, Zoerb C, Jajima J, Lommel D, Walker G, Mueller KM, … Bohle RM (2005). Quantification of in-stent restenosis parameters in rabbits by micro-CT. Fortschr Geb Rontgenstr Nuklearmed, 177, 501–506. 10.1055/s-2005-858055

Loos A, Rohde R, Haverich A, & Barlach S (2007). In vitro and in vivo biocompatibility testing of absorbable metal stents. Macromolecular Symposia, 253, 103–108.

Molyneux AJ, Birks J, Clarke A, Sneade M, & Kerr RS (2015). The durability of endovascular coiling versus neurosurgical clipping of ruptured cerebral aneurysms: 18 year follow-up of the UKcohort of the international subarachnoid aneurysm trial (ISAT). Lancet, 385(9969), 691–697. [PubMed: 25465111]

Opie NL, van der nagel NR, John SE, Vessey K, Rind GS, Ronayne SM, … Oxley TJ (2017). Micro-CT and histological evaluation of an neural interface implanted within a blood vessel. IEEE Transactions on Biomedical Engineering, 64(4), 928–934. [PubMed: 27337706]

Rodriguez JN, Clubb FJ, Wilson TS, Miller MW, Fossum TW, Hartman J, … Maitland DJ (2014). In vivo response to an implanted shape memory polyurethane foam in a porcine aneurysm model. Journal of Biomedical Materials Research. Part A, 102, 1231–1242. [PubMed: 23650278]

Rodriguez JN, Hwang W, Horn J, Landsman TL, Boyle A, Wierzbicki MA, & Maitland DJ (2015). Design and biocompatibility of endovascular aneurysm filling devices. Journal of Biomedical Materials Research. Part A, 103(4), 1577–1594. [PubMed: 25044644]

Rousselle S, & Wicks J (2008). Preparation of medical devices for evaluation. Toxicologic Pathology, 36, 81–84. [PubMed: 18337224]

Velnar T, Bailey T, & Smrkolj V (2009). The wound healing process: An overview of the cellular and molecular mechanisms. The Journal of International Medical Research, 37(5), 1528–1542. [PubMed: 19930861]

Wierzbicki MA, Bryant J, Miller MW, Keller B, & Maitland DJ (2016). Mechanical and in vitro evaluation of an experimental canine patent ductus arteriosus occlusion device. Journal of the Mechanical Behavior of Biomedical Materials, 59, 156–167. [PubMed: 26766327]

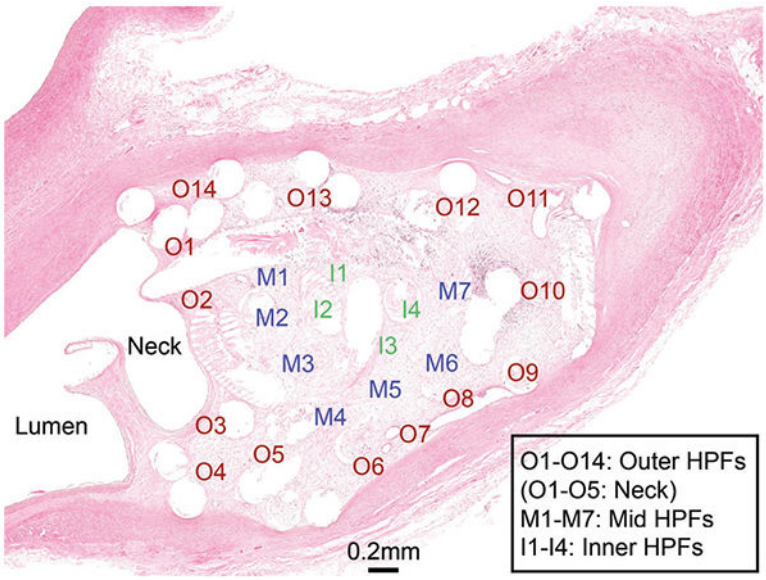

FIGURE 1.

Aneurysm cross-section with HPFs denoted. Each HPF was analyzed for numbers of inflammatory cells present. I, inner region; M, mid region; O, outer region

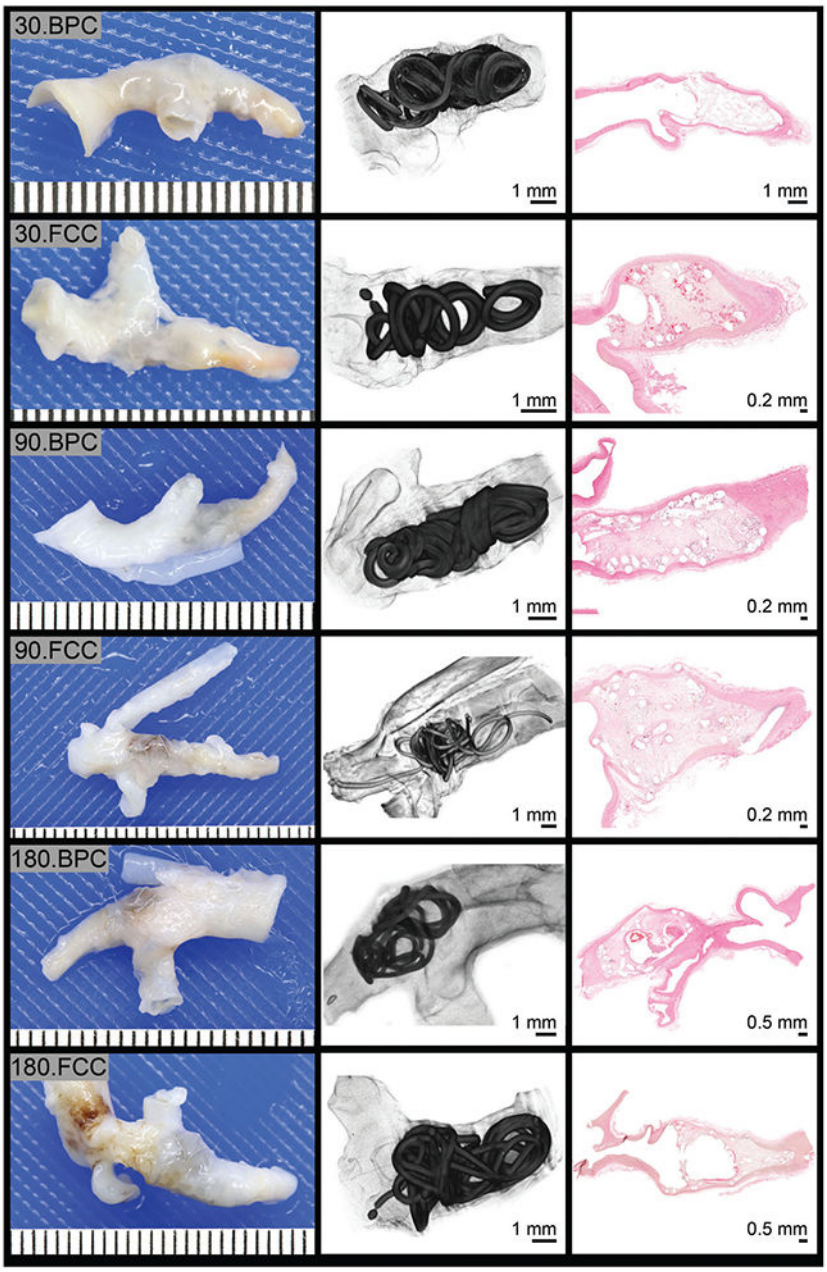

FIGURE 2.

Gross, micro-CT and histology images from aneurysms at 30, 90, and 180 days postexplant

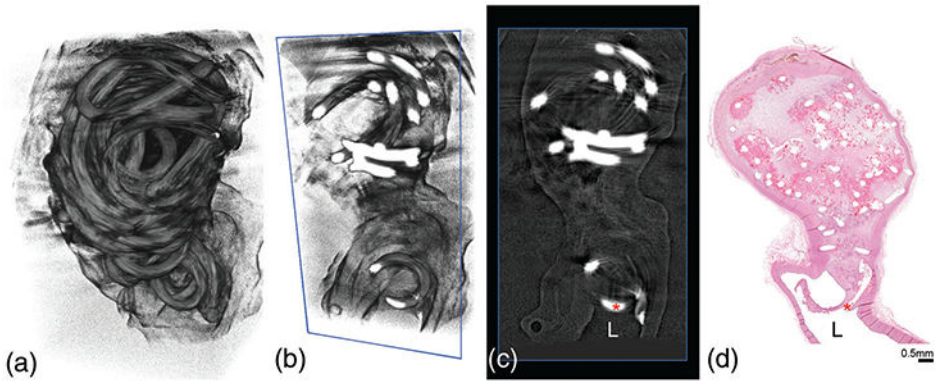

FIGURE 3.

Micro-CT correlation with histology to confirm presence of coil in parent artery lumen. The 3D reconstruction of aneurysm filled with occlusion device (a) can be viewed in axial slices (b, c) to confirm if coils (red asterisk) are present in the parent artery lumen (L), which can then be correlated with the mid-sagittal H&E stained cross-section (d)

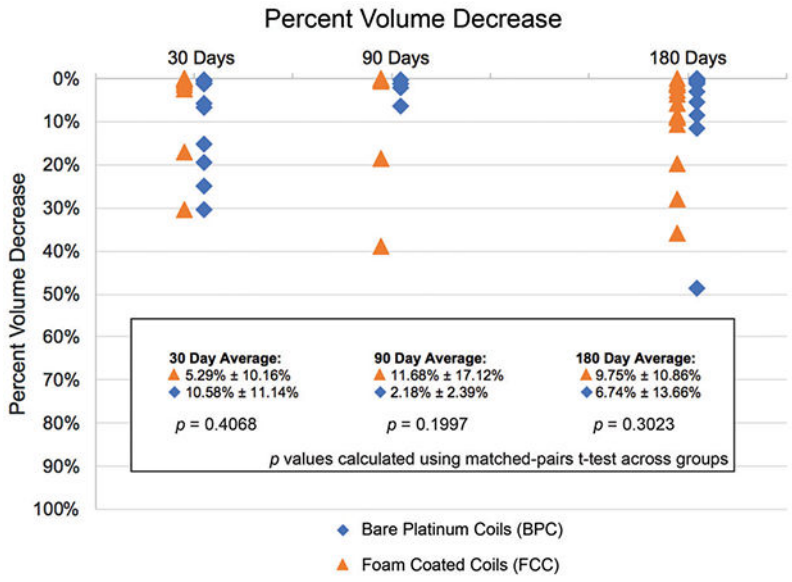

FIGURE 4.

Percent decrease in aneurysm volume per time point relative to the aneurysm volume at implant

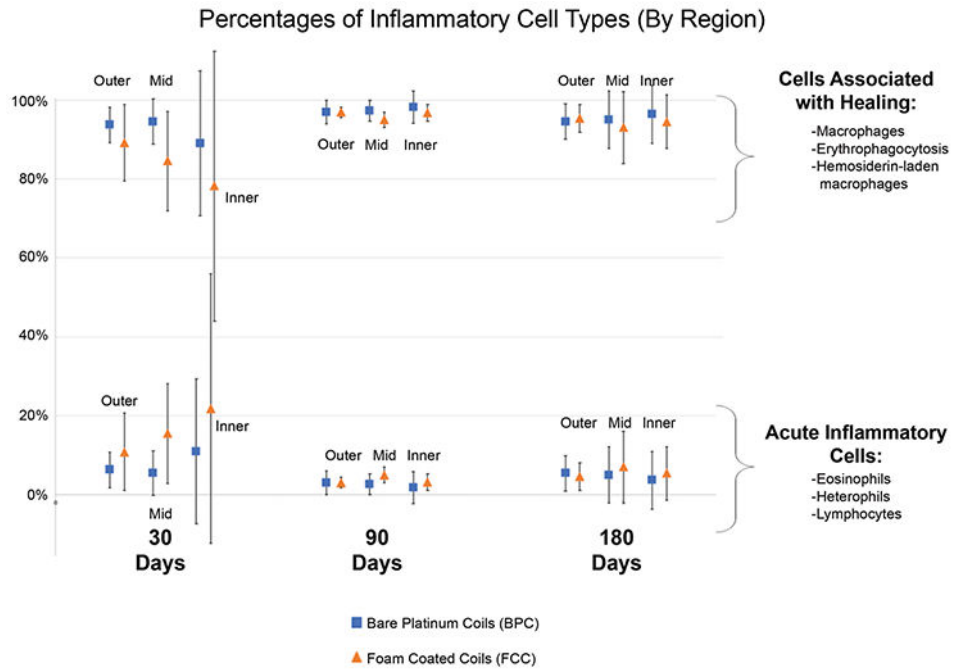

FIGURE 5.

Percentages of inflammatory cell types by region and device type broken down into cells typically associated with healing (macrophages, erythrophagocytosis, and hemosiderin-laden macrophages), and cells typically associated with acute inflammation (eosinophils, heterophils, and lymphocytes). Inflammation totals are defined in Table 3

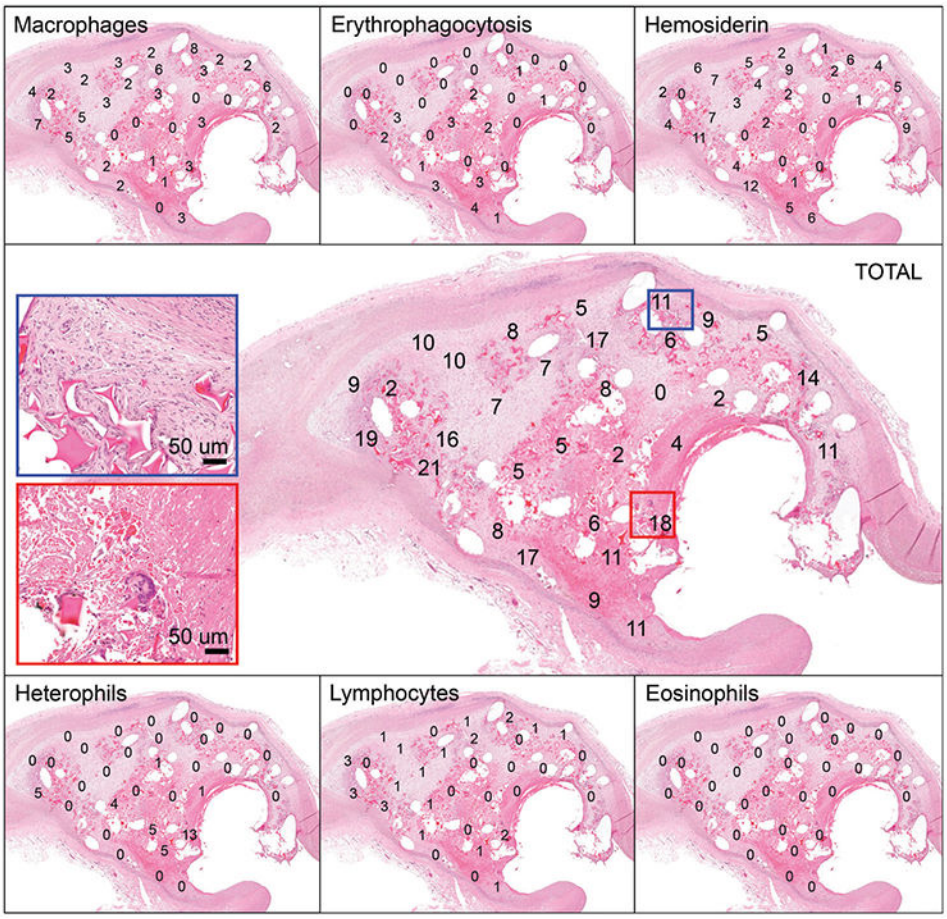

FIGURE 6.

Histology slide of aneurysm cross-section with cell counts displayed. Each panel depicts the same cross-section of an aneurysm, with the number of a specific cell type counted within a high power field (HPF) displayed. Each number within the panels along the top and bottom represents the number of that specific inflammatory cell type indicated (i.e., macrophage, erythrophagocytosis, hemosiderin-laden macrophage, heterophil, lymphocyte, or eosinophil) counted in that HPF. In this example, there are 32 HPFs examined. The panel in the middle represents the total number of inflammatory cells counted in each HPF (i.e., each number represents the sum of all cell types counted for that HPF from other panels). The blue rectangle indicates an HPF along the outer region that had increased numbers of macrophages (8/11 cells counted). The red rectangle indicates an area along the aneurysm neck with increased heterophils present (13/18 cells counted)

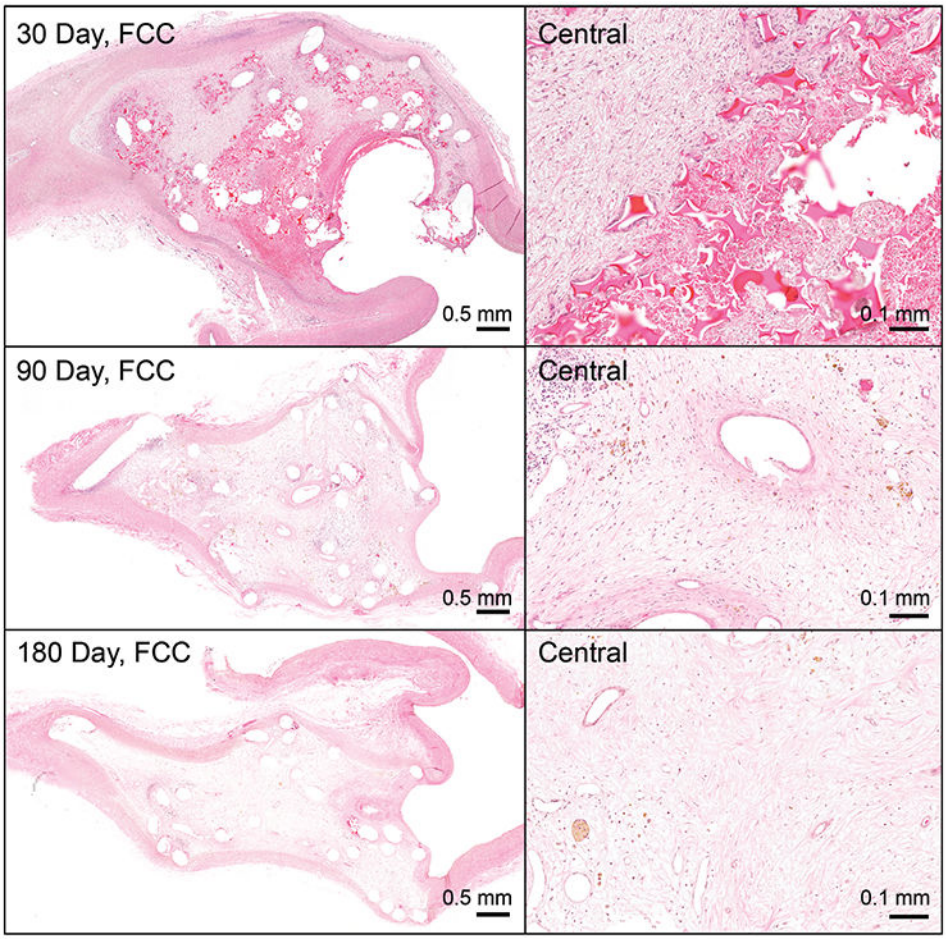

FIGURE 7.

Foam-coated coil (FCC)-treated aneurysms at 30, 90, and 180 days. Central regions progress from abundant foam present with cellular infiltration (mostly of macrophages, but some acute inflammatory reaction), to minimal foam at 90 days with cellular activity but more deposition of fibrin/collagen, to finally at 180 days, primarily a healing response consisting of moderate collagen deposition and more hemosiderin laden macrophages. (Overview pictures: scale bar = 0.5 mm; Central pictures: scale bar = 0.1 mm)

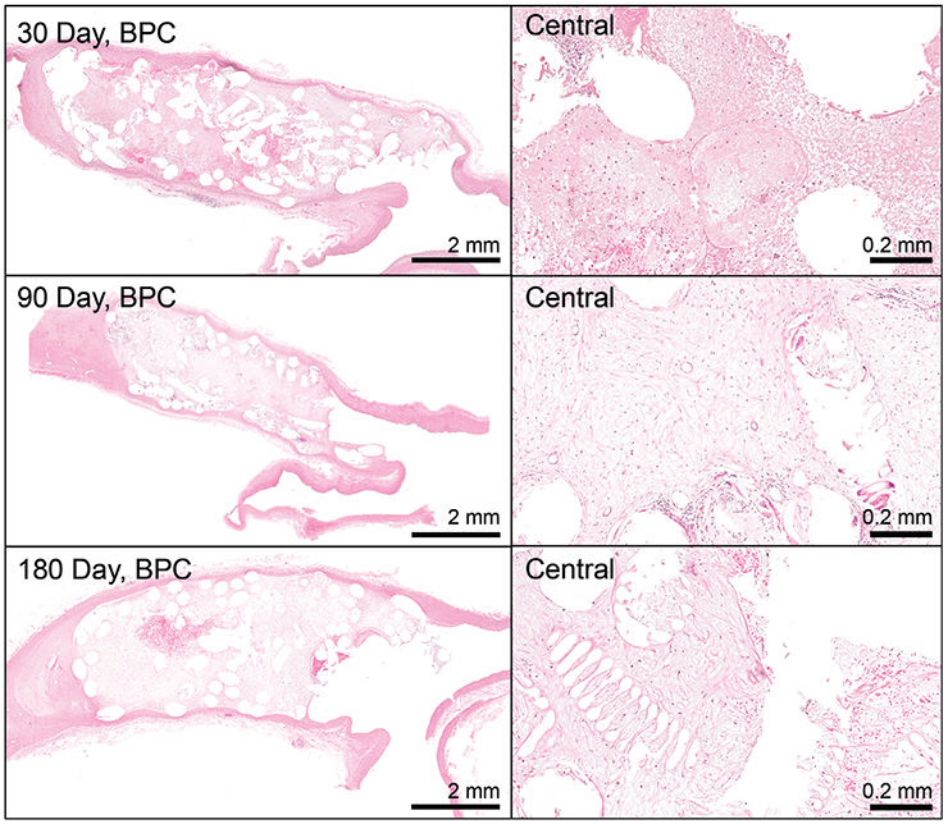

FIGURE 8.

Bare platinum coils (BPC)-treated aneurysms at 30, 90, and 180 days. Central regions exhibit increased cellular infiltration (mostly of macrophages, but some acute inflammatory reaction) into a fibrin extracellular matrix at 30 days. At 90 days, the extracellular matrix is mostly a collagen matrix, which transitions to a slightly more dense matrix at 180 days. (Overview pictures: scale bar = 2 mm; Central pictures: scale bar = 0.2 mm)

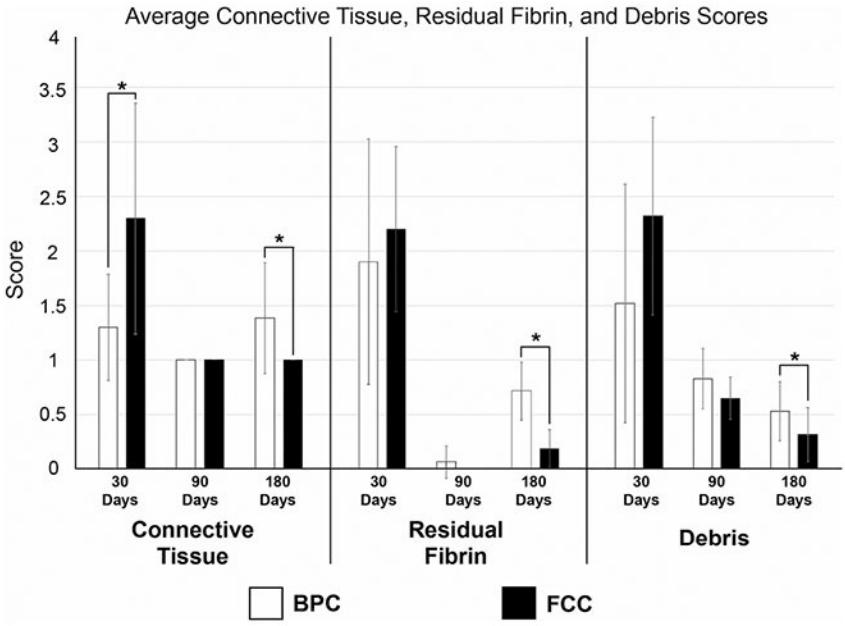

FIGURE 9.

Average Connective Tissue, Residual Fibrin, and Debris Scores per device type per time point. The scoring system is defined in Table 2. Lower scores indicate the preferred outcome in all categories (i.e., less residual fibrin, increased connective tissue coverage, and no to minimal debris present)

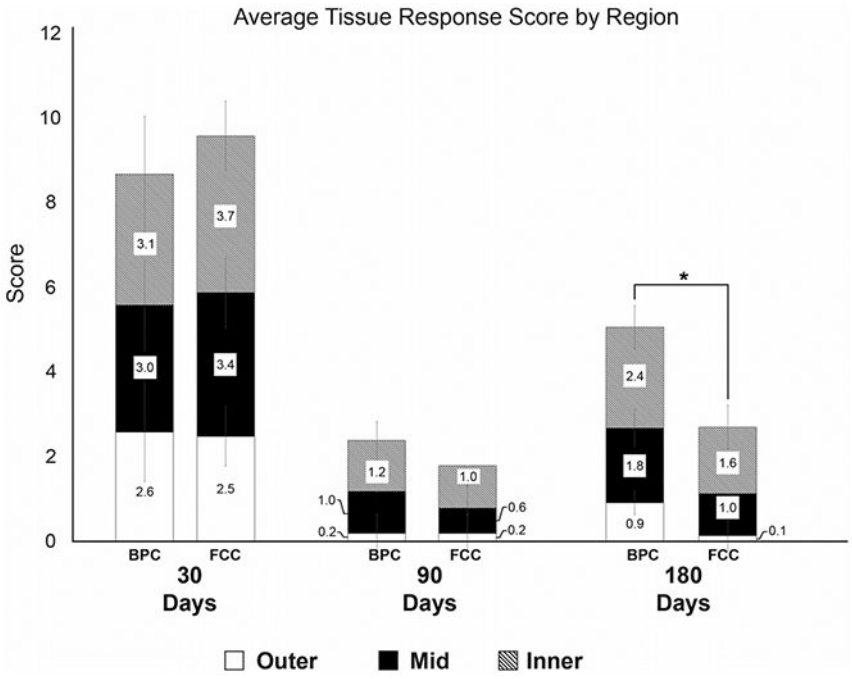

FIGURE 10.

Average tissue response scores of each device type by region. Tissue response scores are defined in Table 4. Tissue response scores are on a 0–6 scale where lower scores are better

TABLE 1

Animal study design

	Number of specimens	
Time point	**Test article (FCC)**	**Control (BPC)**
30 days	*n* = 10	*n* = 10
90 days	*n* = 5	*n* = 5
180 days	*n* = 14	*n* = 12

TABLE 2

Extracellular matrix assessment

Residual fibrin score[a]	Connective tissue score[a]	Debris score[b]
		0: None
1: 0–10%	1: 75–100%	1: Minimal (<5% area covered)
2: 11–25%	2: 50–75%	2: Mild (2–25% area covered)
3: 26–50%	3: 25–49%	3: Moderate (25–50% area covered)
4: >50%	4: 0–24%	4: Severe (>50% area covered)

[a] Assessed using trichrome-stained slides.

[b] Assessed using H&E-stained slides.

J Biomed Mater Res B Appl Biomater. Author manuscript; available in PMC 2021 July 01.

TABLE 3

Inflammation assessment

Cell types counted per HPF*	***HPF = high power field. Defined as 0.01 mm^2.**
C1: Heterophils	
C2: Lymphocytes	
C3: Eosinophils	
C4: Macrophages	
C5: Erythrophagocytosis	
C6: Hemosiderin-laden macrophages	
Inflammation totals	***Inflammation score***
I_T: Inflammation (total) = average total number of cells (*C1–C6*) per HPF	0: $I_x = 0$
	1: $I_x \leqq 1$
	2: $1 < I_x \leqq 4$
I_M: Inflammation (modified) = average total number of cells (*C1–C3*) per HPF	3: $4 < I_x \leqq 8$
	4: $I_x > 8$

TABLE 4

Tissue response score (Jessen et al., 2019)

Score	Definition	Description
0	Healed	Fibrocytes and collagen, multinucleated giant cells; capillaries; dense cellular connective tissue (dominant)
1	Mid-stage healing to healed	Capillaries; multinucleated giant cells; islands of loose matrix and dense collagen
2	Mid-stage healing	Macrophages (hemosiderin laden, cellular and substrate debris), fibroblasts, lymphocytes and admixture substrate (collagen and isolated fibrin fragments), multinucleated giant cells; admixture of neovascular buds and capillaries (dominant); loose cellular connective tissue
3	Early to mid-stage healing	Neovascular buds and capillaries; multinucleated giant cells; admixture of loose collagen (dominant) and fibrin
4	Early stage healing	Macrophages (erythrophagocytosis, cellular and substrate debris phagocytosis), fibroblasts, neutrophils, eosinophils, lymphocytes, multinucleated giant cells, plasma cells; neovascular buds; granulation tissue; admixture of fibrin and loose collagen
5	Residual blood to early stage healing	Neovascular buds; admixture of fibrin (dominant) and loose collagen
6	Residual blood	Cells and fibrin/protein; no vasculature; fibrin, no collagen

TABLE 5

Inflammatory cell counts and inflammation scores

Device type	Average total no. of inflammatory cells per HPF[a] (I_T)	Total inflammation score	Modified cell average[b] (I_M)	Modified inflammation score
Bare platinum coil				
30 day	6.32 ± 1.97	3.00 ± 0.47	0.35 ± 0.23	1.00 ± 0.00
90 day	5.44 ± 2.55	3.00 ± 0.71	0.20 ± 0.23	0.8 ± 0.45
180 day	5.15 ±2.68	2.77 ± 0.6	0.31 ± 0.36	1.08 ± 0.28
Foam coated coil				
30 day	5.44 ± 2.61	2.70 ± 0.82	0.62 ± 0.56	1.1 ± 0.32
90 day	9.72 ± 1.85	3.80 ± 0.45	0.36 ± 0.16	1 ± 0.00
180 day	5.54 ± 0.99	2.93 ± 0.27	0.31 ± 0.30	1 ± 0.39

[a]Value for each aneurysm calculated by the following formula: (heterophils + lymphocytes + eosinophils + macrophage + erythrophagocytosis + hemosiderin-macrophages)/(total number of high power fields examined).

[b]Modified cell average for each aneurysm calculated by the following formula: (heterophils + lymphocytes + eosinophils)/(total number of high power fields examined).